Magnetodipolar interlayer interaction effect on the magnetization dynamics of a trilayer square element with the Landau domain structure

D. V. Berkov[a] and N. L. Gorn[a]
Innovent Technology Development, Prüssingstr. 27b, D-07745 Jena, Germany

(Received 10 December 2007; accepted 2 January 2008; published online 10 March 2008)

We present a detailed numerical simulation study of the effects caused by the magnetodipolar interaction between ferromagnetic (FM) layers of a trilayer magnetic nanoelement on its magnetization dynamics. As an example, we use a $Co/Cu/Ni_{80}Fe_{20}$ element with a square lateral shape where the magnetization of FM layers forms a closed Landau-like domain pattern. First, we show that when the thickness of the nonmagnetic (NM) spacer is in the technology relevant region $h \sim 10$ nm, magnetodipolar interaction between 90° Neel domain walls in FM layers *qualitatively* changes the *equilibrium* magnetization state of these layers. In the main part of the paper, we compare the magnetization *dynamics* induced by a sub-nsec field pulse in a single-layer $Ni_{80}Fe_{20}$ (Py) element and in the Co/Cu/Py *trilayer* element. Here, we show that (i) due to the spontaneous symmetry breaking of the Landau state in the FM/NM/FM trilayer, its domains and domain walls oscillate with different frequencies and have different spatial oscillation patterns; (ii) magnetization oscillations of the trilayer domains are strongly suppressed due to different oscillation frequencies of domains in Co and Py; (iii) magnetization dynamics qualitatively depends on the relative rotation sense of magnetization states in Co and Py layers and on the magnetocrystalline anisotropy kind of Co crystallites. Finally, we discuss the relation of our findings with experimental observations of magnetization dynamics in magnetic trilayers, performed using the element-specific time-resolved x-ray microscopy. © *2008 American Institute of Physics*. [DOI: 10.1063/1.2890397]

I. INTRODUCTION

Studies of nanoelements patterned out of magnetic multilayers constitute now a rapidly growing research area due to their already existing and very promising future applications. Using modern patterning technologies, it is possible to produce arrays of nanoelements with lateral sizes of $\sim 10^2 - 10^3$ nm and nearly arbitrary shapes. Such elements and their arrays can be employed in magnetic random access memory (MRAM) cells, miniaturized magnetoresistance sensors (in read/write hard disk heads), advanced high-density storage media, spintronic devices,[1] etc.

Small lateral sizes of these single- and multilayered structures lead to qualitatively new features of their magnetization dynamics, with the quantization of their spin wave eigenmodes being the most famous example (see, e.g., Refs. 2–5). Thorough understanding of this novel features is crucially important both for the progress of the fundamental research in this area and for the development of reliable high-technology products based on such systems.

In the past decade, extensive experimental and theoretical efforts were dedicated to the studies of magnetization dynamics of *single*-layer nanoelements. Among them, the nanodisks possessing closed magnetization configuration with the central vortex (for continuous disks) or without it (for rings with the hole in the middle) represent the simplest nontrivial example due to their circular form and hence axially symmetric magnetization configuration. Magnetization dynamics of these nanodisks has been extensively studied using advanced experimental techniques, analytical theories, and numerical simulations[6] and is satisfactory understood.

The next complicated case is a square or rectangular single-layer nanoelement with either saturated magnetization state or closed Landau domain structure. In the state close to saturation, the main nontrivial effect is due to the strong demagnetizing field near the element edges perpendicular to the field and magnetization direction; corresponding dynamics could also be understood quantitatively combining experimental and theoretical methods (see, e.g., Refs. 2 and 4 and references therein). The closed Landau magnetization pattern is much more demanding at least from the theoretical point of view because magnetization dynamics of this structure exhibits both highly localized (oscillation of the central core and domain walls) and extended (oscillation of domain areas) modes. However, many important features of this dynamics could be also understood very recently using such advanced experimental methods as time-resolved Kerr microscopy and space resolved quasielastic Brillioin light scattering techniques, supported by detailed numerical simulations.[7–11]

However, single-layer elements are not very interesting from the point of view of potential applications because almost any technical device based on magnetic nanolayers employs—for various but fundamental reasons—mainly multilayer structures. An additional layer (or several such layers) is required, e.g., as a reference layer with "fixed" magnetization to detect via some magneto resistance (MR) effect the resistance change when the "free" layer changes its magnetization direction, or as an electron spin polarizer in spintronic devices, etc. For this reason the magnetization dy-

[a]Electronic mail: db@innovent-jena.de.

namics of *multilayered* structures is of the major interest.

In such structures, the interlayer interaction effects play often a very important role. Even if we leave aside a strong exchange (RKKY) coupling present in structures with very thin nonmagnetic spacers consisting of some specific materials such as Ru, we are still left with the unavoidable magnetodipolar coupling between the layers. This coupling is identically zero only for a multilayer structure with infinitely extended and homogeneously magnetized layers—the situation which is virtually never encountered in practice. For this reason, understanding of the magnetodipolar interlayer interaction influence is absolutely necessary for further progress.

This interaction is especially strong in situations, where the layer magnetization is—at least in some regions—perpendicular to the free layer surface, thus inducing very large "surface magnetic charges" and consequently—high stray fields. Typical example of such systems is multilayers with a perpendicular magnetic anisotropy and nanoelements where the magnetization lies in the layer plane, but is nearly saturated, so that large stray fields emerge near the side edges of a multilayer stack. The influence of the interlayer interaction in such systems has been extensively investigated in the past for the quasistatic magnetization structures (see, e.g., the review[12] and references therein) and very recently—by studies of the magnetization dynamics.[13]

To avoid the strong interaction caused by the magnetization directed normally to the free surface, a commonly used idea is to employ multilayer nanoelements with closed magnetization structures. In nanodisks, such a structure is represented by an in-plane rotating magnetization, containing a central vortex as the only element producing strong demagnetizing field. Magnetodipolar interaction between the cores of such vortices in such multilayered circular nanodots has been investigated recently in Ref. 13.

For the next commonly used nanoelement shape—magnetic rectangle—the closed magnetization structure is achieved by the famous Landau pattern with four homogeneously magnetized domains and four 90° domain walls (in the case of a square element). For sufficiently thin films commonly used in technologically relevant systems these walls are the so called Néel walls[14] with the magnetization lying almost in the element plane. Such a magnetization configuration contains only volume "magnetic charges" (no free poles on the element surface, and hence—no surface charges), which are usually weaker than surface charges. For this reason, the interlayer interaction mediated by the domain walls is multilayer elements with the closed magnetization structure is expected to be weaker than in multilayer stacks with saturated magnetization.

However, recently, several research groups[15–18] have demonstrated that the stray field caused by the magnetization of vortex and/or Néel walls in one layer of a multilayered system can still strongly affect the magnetic state of other layers. Most of these studies use simplified domain wall (DW) models which enable a semianalytical treatment of the problem (see, e.g., Ref. 15 and 16), but rigorous micromagnetic simulations have confirmed that the stray field of a vortex wall with the Neel cap[17] or of a purely Néel wall[18] can strongly affect the magnetic state of other layers even if the interlayer separation is as large as ~100 nm.[18]

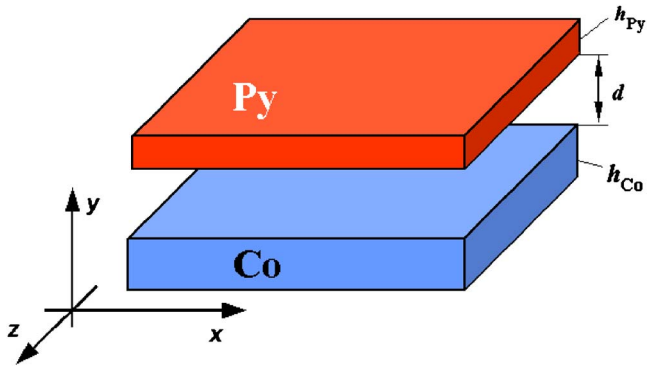

FIG. 1. (Color online) Geometry of the simulated system, coordinate axes, and the pulsed field direction used in simulations.

In this study, we consider multilayer square elements with lateral sizes ~1 m km and thicknesses of magnetic layers and nonmagnetic spacers ~10 nm (i.e., geometry typical for numerous applications). We shall demonstrate that in such systems the magnetodipolar interlayer interaction due to the Néel domain walls of the closed Landau structure is strong enough to change qualitatively both the *quasistatic* magnetization structure and magnetization *dynamics* of a system. The paper is organized as follows. After the brief description of our simulation methodology (Sec. II A), we show reference results for a square single-layer element which will serve for comparison with multilayered systems. Afterward we analyze in detail the effect of the interlayer interaction on the quasistatic magnetization structure and magnetization dynamics for a square FM/NM/FM trilayer (Sec. II C), considering both the influence of the initial magnetization state—compare Secs. II C and II D, and the effect of the random polycrystalline grain structure—compare Secs. II D and II E. In Sec. III, we compare our results with (unfortunately very few) available experimental and numerical studies of similar systems, and discuss the possibility of an experimental verification of our simulation predictions.

II. NUMERICAL SIMULATION RESULTS

A. Numerical simulations setup

In this study, we have simulated the trilayer element Co/Cu/Py with the following geometry shown in Fig. 1 (when not stated otherwise): lateral sizes 1×1 m km^2, Co and Py layer thicknesses $h_{Co}=h_{Py}=25$ nm, Cu interlayer thickness (nonmagnet spacer thickness between Co and Py layers) $h_{sp}=10$ nm. Both magnetic layers were discretized into $N_x\times N_z\times N_y=200\times200\times4$ rectangular prismatic cells. We have checked that the discretization into at least four in-plane sublayers was necessary to reproduce correctly the three-dimensional (3D) magnetization structure of 90° DWs present in the equilibrium Landau magnetization state of square nanoelements.

The following magnetic parameters have been used: for Py-saturation magnetization $M_S^{Py}=860$ G, exchange stiffness constant $A^{Py}=1\times10^{-6}$ erg/cm and cubic magnetocrystalline grain anisotropy $K_{cub}^{Py}=5\times10^3$ ergs/cm^3; for Co-M_S^{Co}

$=1400$ G, $A^{Co}=3\times10^{-6}$ erg/cm and magnetocrystalline grain anisotropies $K_{cub}^{Co}=6\times10^5$ ergs/cm^3 for the cubic fcc modification of Co and $K_{un}^{Co}=4\times10^6$ ergs/cm^3 for its uniaxial hcp modification (see, Ref. 19 for discussion of all values for Co). The average grain (crystallite) size $\langle D\rangle=10$ nm (in all directions) with 3D randomly oriented anisotropy axes of various crystallites was used for both magnetic materials. There was no correlation between the crystallites in Py and Co layers.

Simulations of both the equilibrium magnetization structure and magnetization dynamics were performed using our commercially available MICROMAGUS package (see, Ref. 20 for implementation details). For simulations of the magnetization dynamics, the package employs the optimized Bulirsch–Stoer method with the adaptive step-size control to integrate the Landau–Lifshitz–Gilbert equation for the magnetization motion with the standard linear Gilbert damping (damping constant was set to $\lambda=0.01$ throughout our simulations). Due to the small amplitude of magnetization oscillations studied here, we believe that this simplest damping form adequately describes the energy dissipation in our system. We also did not take into studies additional damping caused by the spin pumping effect in magnetic multilayers (see, e.g., Ref. 21) because this is beyond the scope of this paper.

We have studied magnetization dynamics of our system in a *pulsed* magnetic field applied *perpendicularly* to the element plane. To obtain magnetization excitation *eigenmodes* of an equilibrium magnetization state, we have applied a short field pulse in the out-of-plane direction with the maximal field value $H_{max}=100$ Oe and the trapezoidal time dependence with rise and fall times $t_r=t_f=100$ ps and the plateau duration $t_{pl}=300$ ps. To obtain the eigenmode spectrum, we have set the dissipation constant to zero ($\lambda=0$) and recorded magnetization trajectories of each cell during the pulse and for $\Delta t=10$ ns after the pulse was over. Spatial profiles of the eigenmodes (spatial maps of the oscillation power distribution in the element plane) were then obtained in the meanwhile standard way[2,22] using the Fourier analysis of these magnetization trajectories after the pulse decay. Because the applied field pulse was spatially homogeneous, we could observe only eigenmodes which symmetry was not lower than the symmetry of the equilibrium magnetization state of the studied system. In principle, the analyses of the eigenvalues and eigenvectors of the energy Hessian matrix[23] allow us to obtain all eigenmodes, but our method can be used for much larger systems because it does not require the explicit search of eigenvalues for large matrices with sizes $Z\times Z$ proportional to total number of discretization cells $Z\sim N_x\times N_z\times N_y$. For the qualitative analysis of the influence of various physical factors on the magnetization dynamics aimed in this paper, our method provides enough information.

To study the *transient* magnetization dynamics which could be compared to real experiments, we have applied the same field pulse as described above and recorded magnetization time dependencies for each discretization cell during the pulse and for $\Delta t=3$ ns after the pulse. Here, the dissipation constant was set to $\lambda=0.01$—the value commonly reported in literature for thin Py films; the same constant was used for Co layer. We have checked that increasing this value up to $\lambda=0.05$ led, as expected, to faster overall oscillation decay, but did not produce any qualitative changes in the magnetization dynamics.

B. Single layer Py element as the reference system

Keeping in mind that we are going to study interaction effects in a trilayer system, we first present reference results for the single Py nanoelement with the same parameters as the Py layer of the complete trilayer (the square element 1×1 m km^2, with the thickness $h_{Py}=25$ nm, $M_S^{Py}=860$ G, $A^{Py}=1\times10^{-6}$ erg/cm, $K_{cub}^{Py}=5\times10^3$ ergs/cm^3). Figure 2(a) shows the equilibrium magnetization structure of such a nanoelement obtained starting from the initial state consisting of four homogeneously magnetized domains in corresponding triangles [as shown, e.g., in Fig. 4(a)], whereby magnetic moments of four central cells were oriented perpendicular to the layer plane (along the y axis). As expected, the very small random grain anisotropy of Permalloy has virtually no influence on the magnetization state so that the equilibrium magnetization forms a nearly perfect closed Landau magnetization pattern with four 90° Néel domain walls between the domains and the central vortex showing upwards.

Spectrum of magnetization excitations for this Landau pattern is shown in Fig. 2(b) together with spatial maps of the oscillation power of the out-of-plane magnetization component for each significant spectral peak. We remind (see Sec. II A) that the field pulse used to draw the magnetization out of its equilibrium state was spatially homogeneous, and hence only modes with the corresponding symmetry could be excited. Excitation modes of the Landau domain pattern have been recently studied in detail in Refs. 10 and 11, so here we will only briefly mention several issues important for further comparison with the trilayer system.

The lowest peak in the excitation spectrum in Fig. 2(b) corresponds, in a qualitative agreement with the results from Ref. 10, to the domain wall oscillations, whereby due to the spatial symmetry of the exciting field pulse, we observe only the oscillation mode where all domain walls oscillate in phase. We are not aware of any analytical theory which would allow to calculate the frequency of a 90° domain wall oscillations and thus could be compared to our simulations. From the qualitative point of view, DW oscillations are exchange dominated and their frequency is the lowest one among other exchange-dominated magnetization excitations because the equilibrium magnetization configuration inside a DW is inhomogeneous and thus its stiffness with respect to small deviations from the equilibrium is smaller than for a collinear magnetization state.

Peaks with higher frequencies correspond to the oscillations within four triangular domains of the Landau structure; again, only symmetric in-phase oscillations have been observed. According to the analysis performed in Refs. 10 and 11 domain excitations can be classified into the following types. First, there exist modes which power distribution has nodes (between the peaks) in the radial direction, i.e., from the square center to its edges. Corresponding wave vector is

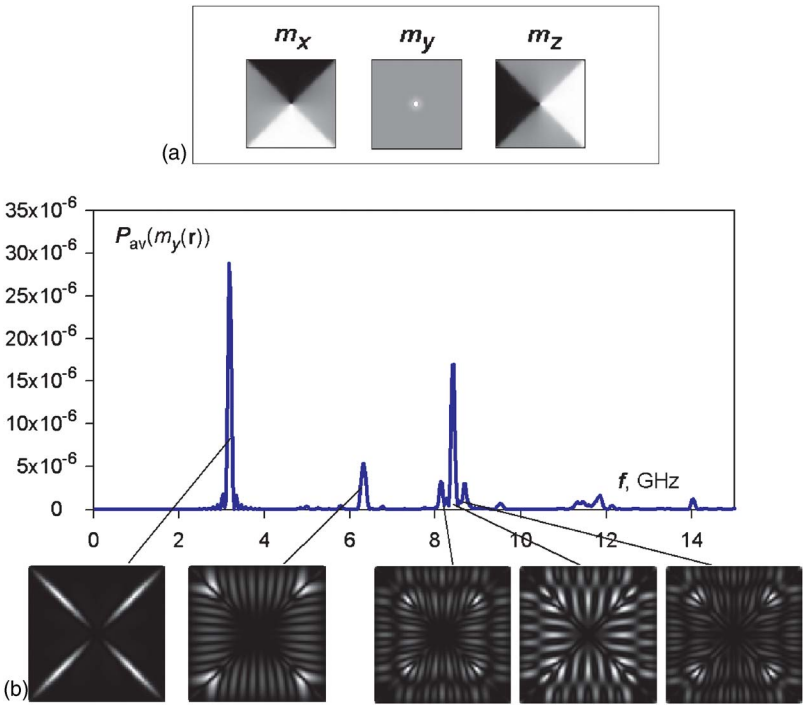

FIG. 2. (Color online) Magnetic properties of the single-layer squared *Permalloy* element ($1000\times1000\times25$ nm^3): (a) equilibrium Landau magnetization structure in zero external field shown as grey scale maps of magnetization projections; (b) spectrum of eigenmodes excited by the small out-of-plane pulsed homogeneous field for the state shown in (a). Gray-scale maps below the spectrum show the spatial distribution of the oscillation power for corresponding peaks (bright areas correspond to a large oscillation power).

perpendicular to the magnetization direction in the domains ($\mathbf{k}\perp\mathbf{M}$). Such modes are similar to Damon–Eshbach modes in extended thin films and are called radial (wave vector in the radial direction) (Ref. 10) or transverse (because $\mathbf{k}\perp\mathbf{M}$).[11] Second, there exist modes with power distribution nodes along the contour around the square center. In this case, regions with high power form elongated bands from the center to the edges of the square. For these modes, the wave vector of their spatial power distribution is roughly parallel to the local magnetization direction in each domain ($\mathbf{k}\|\mathbf{M}$); their behavior is similar to the backward volume modes in extended thin films. For obvious reasons, this second type is called azimuthal[10] or longitudinal[11] modes.

As it can be seen from Fig. 2(b), our field pulse excites mainly an azimuthal mode with the frequency $f\approx3.2$ GHz and several modes which can be classified as mixed radial-azimuthal modes because their spatial power distribution has nodes along both the radial direction and the contours around the square center. Our results can be compared to simulations from Ref. 11, where the Py element with the same lateral sizes 1000×1000 nm^2, but with the smaller thickness $h=16$ nm was studied. Qualitatively, our power maps are very similar to those shown in Ref. 11, but there are some important discrepancies. First of all, our overall excitation spectrum is very different from that presented in Ref. 11 [compare our Fig. 2(b) with Fig. 1(d) from Ref. 11], although several peak positions are very close. Our power maps for specific modes also have some qualitative similarities to several maps presented in Ref. 11, but detailed comparison does not make much sense due to the different total power spectra as mentioned above. All these differences may arise because the simulated nanoelement in Ref. 11 was not discretized in the layer plane, but we believe that the major reasons are (i) the much shorter excitation pulse ($t_d=2.5$ ps pulse length) used in Ref. 11 compared to our (300 ps) and (ii) the presence of the finite damping in simulations from Ref. 11. This problem requires further investigation, but is beyond the scope of this paper.

Transient magnetization dynamics for the single-layer Py element after the application of the same field pulse as used for the studies of the excitation spectrum is shown in Fig. 3. We remind that for these simulations, we have used the nonzero damping $\lambda=0.01$ typical for Py films. Figure 3 shows the time dependence of the angle between the average layer magnetization and the element plane $\Psi(t)\sim m_\perp(t)$ [panel (a)], spatial maps of the out-of-plane magnetization projection during the pulse (b) and after the pulse (c). By displaying the out-of-plane magnetization projection, we have subtracted the equilibrium magnetization $\mathbf{m}^{eq}(\mathbf{r})$ so that maps in Fig. 3 (and all other figures where the transient magnetization dynamics is shown) represent the difference $\Delta m_\perp=m_\perp(\mathbf{r},t)-m_\perp^{eq}(\mathbf{r})$. Homogeneous gray background around the magnetic element shows the reference grey intensity for $\Delta m_\perp=0$.

First of all, we emphasize that even the small damping $\lambda=0.01$ used here leads to relatively fast oscillation decay (within ~3 ns after the pulse). After the initial increase of the perpendicular magnetization projection due to the field pulse [see the bright contrast across the whole square in Fig. 3(b)] is over, the time dependence of the average magnetization is dominated by relatively fast oscillations of the domains, slightly modulated by oscillations of a lower frequency due to the domain wall motion. Corresponding patterns can be seen in Fig. 3(c), where one can directly recognize that domain walls and domains themselves oscillate with very different frequencies. Further, comparison of the time-dependent maps from Fig. 3(c) with the spatial power maps in Fig. 2(b) shows the qualitative relation between the eigenmodes and the transient dynamics of the Py square in this case: not only the contrast due to the DW

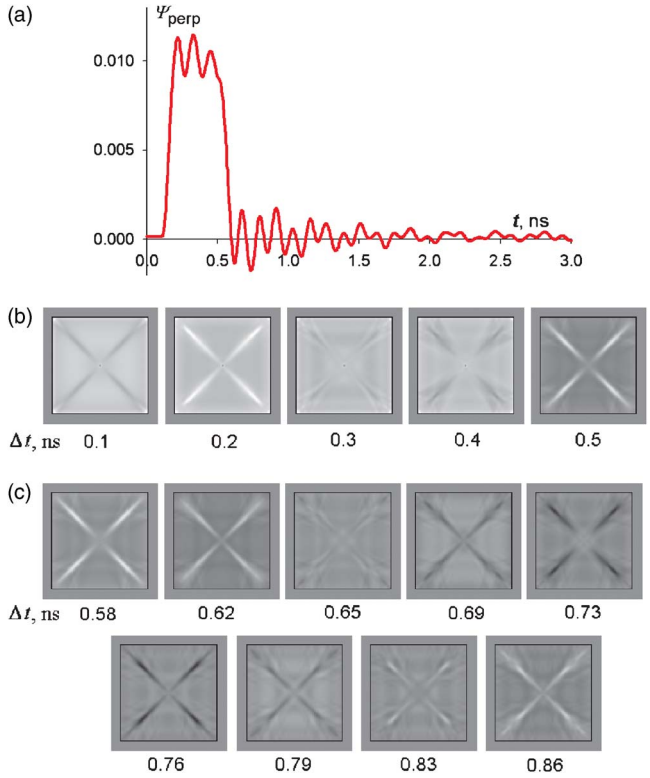

FIG. 3. (Color online) Magnetization dynamics of a single-layer Permalloy element with the same sizes as in Fig. 2 in the pulsed out-of-plane field: (a) time dependence of the angle Ψ_{perp} between the average layer magnetization and the element plane ($\Psi_{perp} \sim \langle m_y(\mathbf{r}) \rangle$, see Fig. 1); the trapezoidal pulse form is shown at the same panel as thin solid line; (b) gray scale maps of $m_y(\mathbf{r})$ (out-of-plane magnetization projection) during the pulse; (c) gray scale maps of $m_y(\mathbf{r})$ after the pulse. Oscillations of both domain walls and domains themselves are clearly seen.

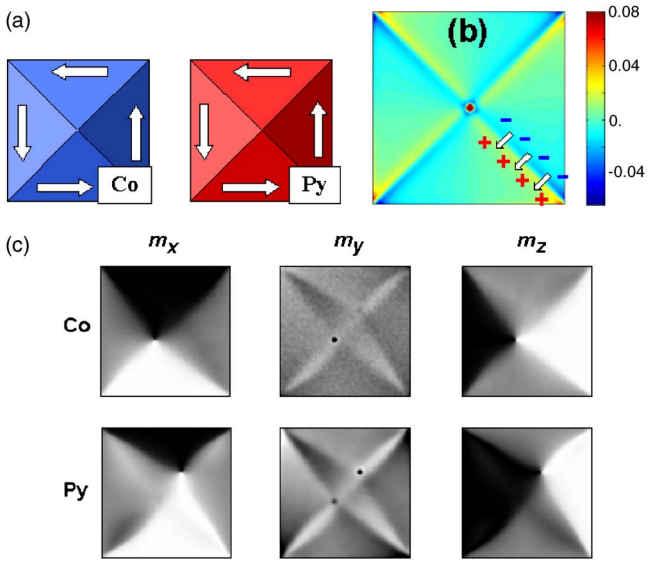

FIG. 4. (Color online) To the formation of a static equilibrium magnetization structure in zero external field for the trilayer Co/Cu/Py element with the lateral sizes 1000×1000 nm^2, Co and Py thicknesses $h_{Co}=h_{Py}=25$ nm and spacer thickness $h_{Cu}=10$ nm. The Co layer possesses a fcc polycrystalline structure with the average crystallite size $\langle D \rangle = 10$ nm and cubic grain anisotropy $K_{cub}=6 \times 10^5$ ergs/cm^3. (a) initial magnetization structure used as the starting state by the calculation of the equilibrium structure shown in (c) as gray scale maps of magnetization projections; (b) initial distribution of the surface charges responsible for the repulsion of 90° domain walls initially located along the main diagonals of the square in Co and Py layers; the color shows the spatial distribution of the out-of-plane magnetization component using the color code displayed in the colorbar on the right.

oscillations but also characteristic wave patterns inside the domains and near the outer regions of domain walls agree qualitatively with the eigenmode power distributions shown in Fig. 2(b).

Analogous simulations (with qualitatively similar results) have been carried out in[24] in order to explain the magnetization dynamics observed there using the time-resolved x-ray microscopy. We shall return to the analysis of these results by comparing our simulation with experimental data in Sec. III.

C. Trilayer Co/Cu/Py element: Landau structures with the same rotation sense in both magnetic layers

1. Deformation of the quasistatic magnetization structure

In this section, we consider the trilayer element Co (25 nm)/Cu (10 nm)/Py (25 nm), 1×1 mkm^2 in-plane size, with magnetic parameters given in Sec. II B and *cubic* random anisotropy of Co grains with $K_{cub}^{Co}=6 \times 10^5$ ergs/cm^3. In order to determine the equilibrium magnetization state of any system by minimizing its magnetic free energy, we have to choose the initial (starting) magnetization state. As such, a state we take in this section for both Co and Py layers the closed in-plane magnetization configuration with sharply formed four triangular domains and four magnetic moments in the middle of each layer pointing in the same out-of-plane direction—along the $+y$ axis (to fix the orientation of the central vortex). An important point is that the rotation sense of the starting magnetization state is *the same* for both layers. This initial state is shown schematically in Fig. 4(a). The situation, when the initial state consists of two closed magnetization configurations with *opposite* rotation senses in Co and Py layers, is considered in the next subsection.

The corresponding equilibrium state which comes out as the result of the energy minimization is shown in Fig. 4(c). The most striking feature of this state is the strong deformation of a "normal" Landau pattern [see Fig. 2(a)]. Namely, central vortices in Co and Py layers are significantly displaced in opposite directions and domain walls are bended—also in opposite directions for Co and Py. Equilibrium domains in both layers do not have anymore a shape of isosceles triangles, but rather form "triangles" with slightly bended sides of different lengths. The degree of the deformation described above depends both on the Cu spacer thickness and the lateral size of the squared trilayer structure (results not shown).

The reason for this unusual deformation can be understood by analyzing the intermediate magnetization configurations arising during the energy minimization. At the first stage of this process, the normal Landau domain configuration inside each layer is formed. It is well known that the 90° Néel domain walls of this magnetization configuration possess both volume and surface "magnetic charges" along them. We consider in detail the configuration of surface charges because the density of these "charges" is simply proportional to the out-of-plane magnetization component

$m_\perp(\mathbf{r})$ and is thus easier to visualize. The corresponding map of the out-of-plane magnetization $m_\perp(\mathbf{r})$ for the equilibrium Landau state of a 25 nm thick square Py nanoelement is shown in Fig. 4(b). One can clearly see significant enhancement of the $m_\perp(\mathbf{r})$ magnitude along all four domain walls. Thus two lines of the opposite "surface magnetic" charges are formed along each wall, building a kind of a "linear dipole" [shown schematically in Fig. 4(b) with arrows and + and − signs]. Now, it is important to realize that the orientation of these dipoles for the given domain wall is the same on *both upper* and *lower* surfaces of the nanoelement. For this reason, for the geometry shown in Fig. 1 and initial magnetization states with the same rotation senses [as shown in Fig. 4(a)], we have on the upper Co surface and lower Py surface linear dipoles with the *same* (parallel) orientations along all four walls in each layer. The volume charges formed due to the nonzero magnetization divergence in the nanoelement volume have a qualitatively similar distribution. They also contribute to the effect described below; with the decrease of the film thickness, when the Néel wall tends to a perfectly "in-plane" magnetization structure, the contribution from these volume charges becomes dominating.

The linear dipoles described above dipoles obviously repel each other, and due to the small interlayer distance (which is in this case significantly smaller than the wall width) this repulsion is very strong. In other words, corresponding 90° Néel domain walls in Co and Py layers "feel" a strong mutual repulsion so that they start to move away from each other. As a result, domain walls in Co and Py layers shift in opposite directions, forming the final equilibrium structure displayed in Fig. 4(c). We note in passing that for the starting state used in these simulations, the central vortices in Co and Py layers have the same orientation and thus attract each other. However, due to the small vortex area, this attraction cannot compensate for the strong repulsion of all domain walls, although the surface density of magnetic charges within the vortices is much higher than along the walls to due a large values of $m_\perp(\mathbf{r})$ within the vortex.

For further consideration, it also important to note that the equilibrium magnetization state of Co is disturbed by its random grain anisotropy more than for the Py layer, for which the influence of this anisotropy is very small. Corresponding disturbance can be seen on the spatial map of $m_\perp(\mathbf{r})$ for Co [Fig. 4(c), middle panel of the upper row], but for the moderate cubic anisotropy of Co $K_{\mathrm{cub}}^{\mathrm{Co}}=6\times10^5$ ergs/cm^3 and the small average crystallite size $\langle D\rangle=10$ nm, this disturbance is still rather weak.

2. Eigenmodes and transient magnetization dynamics

Strong deformation of the equilibrium domain structure discussed in the previous subsection has a qualitative impact on magnetization dynamics in the trilayer as compared to single-layer systems.

First of all, spectrum of eigenmodes of the Py layer from Co/Cu/Py trilayer (shown in Fig. 5, upper panel) is qualitatively different from the corresponding single-layer Py square [Fig. 2(b)]. Irregular domain structure results in a quasicontinuos (for our resolution) oscillation power spectrum because peaks corresponding to the oscillations of each domain and domain wall are located at different positions. In particular, all domain walls oscillate with various frequencies, as shown in Fig. 5 by the peaks of the first group (a, b, c). These peaks can be attributed to oscillations of different domain walls, as displayed on the power spatial maps in the upper row of these maps. Eigenmode frequencies for oscillations within the domains also differ significantly for different Py domains, as shown by the peak positions of the second group in the spectrum. In addition, the power distribution patterns within each domain become highly irregular, as shown by corresponding maps in the second map row in the same figure. For higher frequencies (group 3), the power distribution is even more complicated, although some typical attributes of longitudinal and transverse modes can still be recognized (third map row).

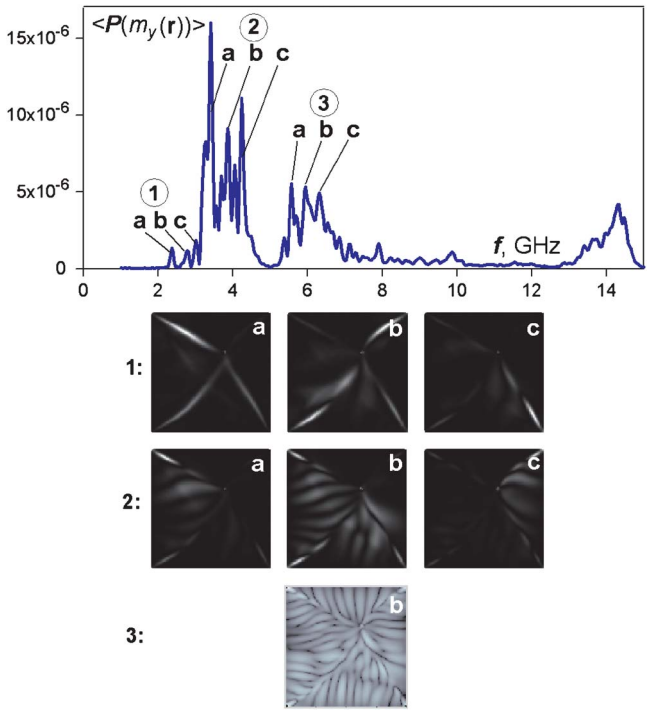

FIG. 5. (Color online) Eigenmodes spectrum for a Permalloy layer of the trilayer element with the static magnetization structure shown in Fig. 4(c). Due to the symmetry breaking of the underlying magnetization state, spectral lines corresponding to the oscillations of different domain walls are positioned at different frequencies (spectral group 1). Spectral peaks corresponding to the domain oscillations form two quasicontinuous groups (groups 2 and 3), whereby each line within a group corresponds to magnetization oscillations within a specific domain, as shown by gray-scale maps of the oscillation power distributions below.

Transient magnetization dynamics of the same trilayer system with the finite damping (it was set to $\lambda=0.01$ for both Co and Py layers) also strongly differs from the monolayer case. Corresponding time dependencies for the out-of-plane angles $\Psi(t)\sim m_\perp(t)$ of the average magnetization are shown in Fig. 6(a) for the Co layer (thin solid line), Py layer (dashed line), and the total system (thick solid line).

The out-of-plane magnetization deviation during the field pulse is smaller for the Co layer than for the Py layer due to the higher saturation magnetization of Co which leads to larger demagnetizing field caused by the out-of-plane ex-

cursion of Co magnetization. Due to the same larger saturation magnetization of Co (and equal Co and Py layer thicknesses), the basic oscillation frequency is now close to the oscillation frequency of domains for the single-layer Co nanosquare: Co layer in the trilayer element determines the overall oscillation frequency, "locking" (capturing) the frequency of the Py layer domains also. Because the eigenfrequencies of Co and Py domains do not coincide, this phenomenon leads to a much faster decay of the domain oscillations in the Py layer compared to the case of the single-layer Py element [compare the dashed lines in Fig. 6(a) to Fig. 3(a)]. In fact, shortly after the pulse is over ($t > 0.6$ ns), Py domain oscillations are barely visible both in the average magnetization time dependence [Fig. 6(a)] and spatial maps of the out-of-plane magnetization component [Fig. 6(c)]. Low-frequency oscillations of the average magnetization of Py are entirely determined by the oscillations of bended DWs. Note that oscillations of different walls are out of phase due to the different eigenfrequencies of the four DWs in the disturbed Landau structure (see Fig. 5) so that for the given time moment different walls (and even different regions of one and the same wall) can exhibit opposite magnetization contrasts as displayed on the last images in both map rows in Figs. 6(b) and 6(c). We shall return to this important circumstance by comparing our simulations to experimental data in Sec. III.

D. Trilayer Co/Cu/Py element: Landau structures with opposite rotation senses in Co and Py magnetic layers

Equilibrium magnetization configuration. It is well known that the initial magnetization state used to start the energy minimization in micromagnetics can have a decisive influence on the equilibrium configuration resulting from this minimization, because any realistic ferromagnetic system possesses many energy minima due to several competing interactions present in ferromagnets. For this reason we have studied the influence of the starting configuration on the equilibrium magnetization and dynamical properties of our trilayer system, choosing as an alternative starting state the same Landau-like domains structure as described at the beginning of Sec. II C 1, but with opposite rotation senses for Co and Py layers [see Fig. 7(a)].

In this case, Landau patterns are also formed at the initial energy minimization stage in both magnetic layers. However, closed magnetization states in Co and Py layers have now opposite rotation senses. For this reason, linear magnetic dipoles appearing along each domain wall at the upper Co and lower Py surfaces, as described in Sec. II C 1 above, are oriented *antiparallel*. Hence, the domain walls (which form these dipoles) attract each other so that these walls become wider and do not move across the layers. This naturally leads to a nearly symmetrical magnetization configurations in both Co and Py. This configuration is qualitatively similar to a "normal" Landau pattern in a single square nanoelement, but domain walls are much broader [compare Figs. 7(b) and 2(a)].

It is instructive to compare the energies of equilibrium magnetization configurations obtained from the two different

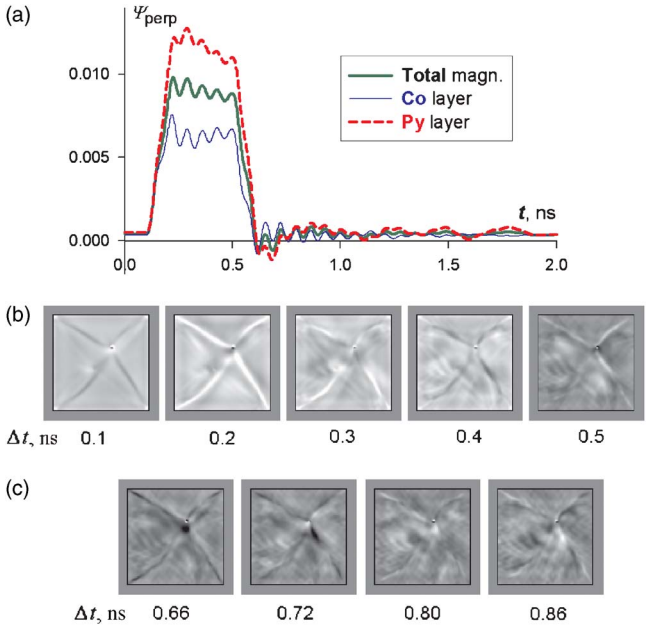

FIG. 6. (Color online) Magnetization dynamics of a trilayer Co/Cu/Py element with the static magnetization structure shown in Fig. 4(c) in the pulsed out-of-plane field: (a) time dependence of the angle Ψ_{perp} between the average magnetization and the element plane for the magnetization of the total element (thick green line), Co layer (thin blue line), and Py layer (thick dashed line). Gray scale maps of the out-of-plane magnetization projection of the Py layer during the pulse (b) and after the pulse (c). Due to different eigenfrequencies, oscillations of different domain walls are out-of-phase here and oscillation of domains themselves are strongly suppressed compared to the case of a single-layered Py element [Fig. 3(c)].

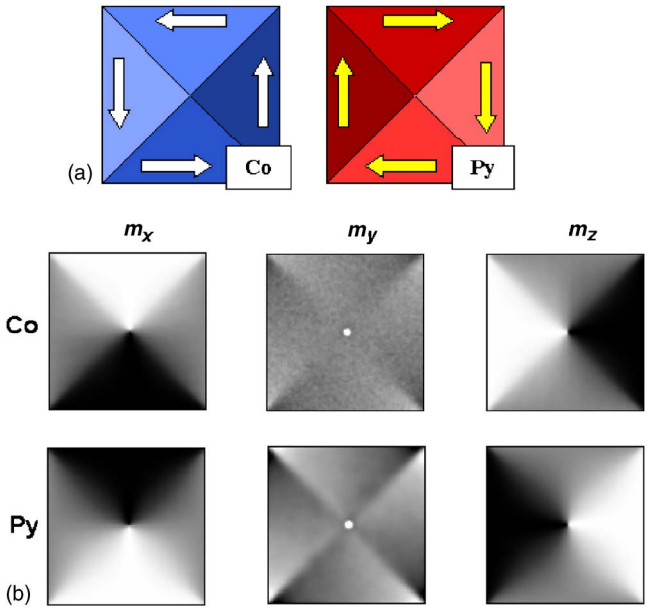

FIG. 7. (Color online) Static equilibrium magnetization structure in zero external field for the same Co/Cu/Py element, as shown in Fig. 4, but starting from Landau magnetization states with opposite rotation senses in Co and Py layers (a). Resulting equilibrium state is shown at panel (b) as gray scale maps of magnetization projections. It can be seen that due to the attraction of domain walls for the starting magnetization states the symmetry of the final equilibrium magnetization structure is nearly preserved.

TABLE I. Energies of equilibrium magnetization states shown in Figs. 4(c) and 7(b).

Initial magnitization state	Total energy (nergs)	Anisotropy energy	Exchange energy	Demagnitization energy
The same rotation senses in Co and Py	4.193	2.851	0.715	0.627
Opposite rotation senses in Co and Py	3.602	2.838	0.510	0.254

starting states, as explained above. From Table I, one can see that the total energy of the configuration with opposite rotation senses of closed magnetization states in Co and Py layers [Fig. 7(b)] is lower than the energy of the state with the same rotation senses in both layers [Fig. 4(c)]. The total energy decrease is mainly due to the smaller exchange energy (wider domain walls) and demagnetizing energy (attraction of domain wall dipoles) in the "opposite" state. However, due to the dominant contribution of the magnetocrystalline anisotropy energy (which is nearly equal in both cases), the total energy difference is not very large, so in experimental realizations, both states can be expected.

Magnetization dynamics: eigenmodes. The almost symmetrical equilibrium magnetization state results in the excitation spectrum with much narrower peaks than for the strongly disturbed asymmetrical state considered in the previous subsection. Corresponding spectrum of eigenmodes for the Py layer (from the Co/Cu/Py trilayer) is shown in Fig. 8 together with spatial maps of the oscillation power. All domain walls have now nearly the same oscillation frequency (similar to the situation for the single-layer Py element), but due to the increased width of the domain walls corresponding oscillation regions are also much wider—compare the first map on Fig. 8 with the first map on Fig. 2(b). Broadening of domain walls manifests itself also in the significant decrease of the corresponding oscillation frequency

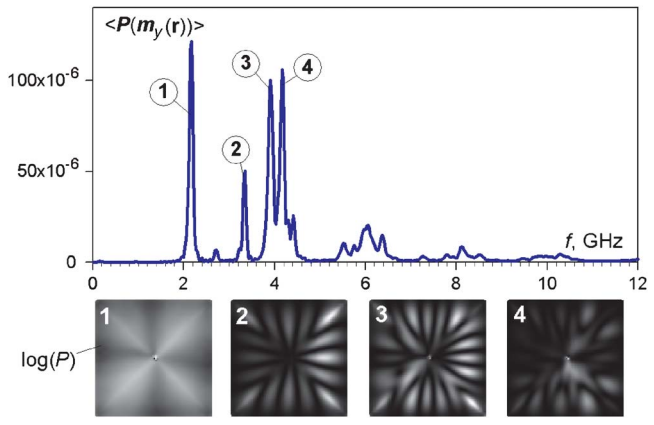

FIG. 8. (Color online) Eigenmodes spectrum for a Permalloy layer of the trilayer element with the static magnetization structure shown in Fig. 7(b). Due to the largely preserved symmetry of domain walls, their oscillations have nearly the same frequency (spectral line 1 and gray-scale map 1). Oscillation power distribution in domain regions (maps 2–4) is still asymmetric due to magnetodipolar interaction with the Co layer which magnetization has a noticeable and spatially varying out-of-plane component due to a significant magnetocrystalline anisotropy (fcc Co).

(≈2.2 GHz for the Py layer within the trilayer versus ≈3.2 GHz for the single-layer Py element).

Spectral peaks corresponding to the oscillations of domains themselves are also much narrower than for the highly asymmetrical state discussed above so that several modes can be well resolved (Fig. 8). Although the oscillation frequencies for various domains coincide (within our resolution $\Delta f \sim 0.1$ GHz) and oscillation power patterns for various domains are very similar (at least for modes 2 and 3 shown in Fig. 8), the absolute values of the spatial power significantly differ from domain to domain. We attribute this effect to the random anisotropy fluctuations of the Co layer. It is well known that due to the small average crystallite size, these fluctuations are largely "averaged out."[25] However, remaining small fluctuations of the out-of-plane magnetization in the Co layer on a large spatial scale have a significant influence on the Py layer eigenmodes due to the large saturation magnetization of Co and small spacer thickness. In particular, these fluctuations may lead to the redistribution of the oscillation power between the domains as it can be seen on the spatial power maps in Fig. 8: the oscillation power in some domains becomes larger, than in the neighbouring domains, even for modes where the spatial power distribution is similar in all domains (see, e.g., second mode in Fig. 8). Another effect of these fluctuations is that despite they are relatively weak, they still can lead to qualitatively different oscillation patterns in different domains for higher modes (e.g., the fourth mode in Fig. 8).

Magnetization dynamics: transient behavior. Due to the qualitatively different equilibrium magnetization states for the trilayer with oppositely oriented Landau structures in Co and Py layers, its transient magnetization oscillations (after the field pulse) for the finite damping case are also very different from both the single-layer square and the trilayer possessing Landau structures with the same rotation senses in both Co and Py layers. Corresponding simulation results are shown in Fig. 9 in the same format, as in Fig. 6.

First of all, due to the largely restored symmetry of the equilibrium magnetization configuration, magnetization oscillations of different domain walls and different domains are now "in phase." Due the much "softer" magnetization configurations of the domains their oscillations have now a much higher amplitude than for the trilayer with "parallel" Landau structures (compare after-pulse oscillations and magnetization maps in Figs. 6 and 9). For this reason, the relative contribution of domain *wall* oscillations to the time dependence of the average magnetization is almost negligible. It can be seen that domain oscillations are dominated by the propagating spin wave which is excited at the square center (core of the Landau structure). Its wavefront has initially a nearly squared form, but when the wave propagates towards the element edges, its front becomes circular. Several nodes appear along this wave front for the sufficiently long propagation time (see several last maps in Fig. 9) in accordance with the spatial power distribution of the system eigenmodes. However, the propagating time shown in Fig. 9 is too short to establish the nodal structure with as many nodes as shown in Fig. 6.

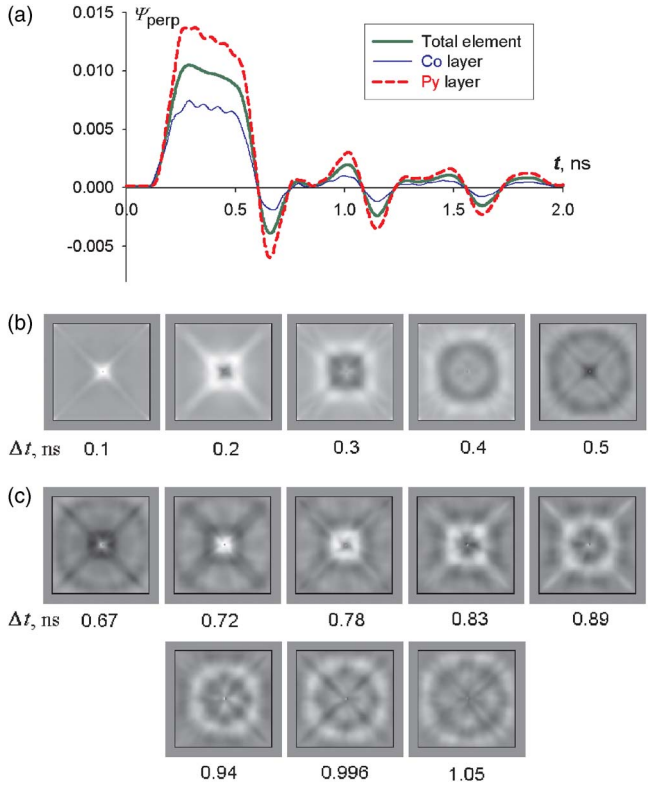

FIG. 9. (Color online) Magnetization dynamics of a trilayer Co/Cu/Py element with the static magnetization structure shown in Fig. 7(b) in the pulsed out-of-plane field presented in the same way as in Fig. 6. It can be seen that the magnetization dynamics is largely dominated by the propagation of the spin wave excited at the central vortex; its wave front has initially the square shape which transforms during the propagation into a nearly circular one.

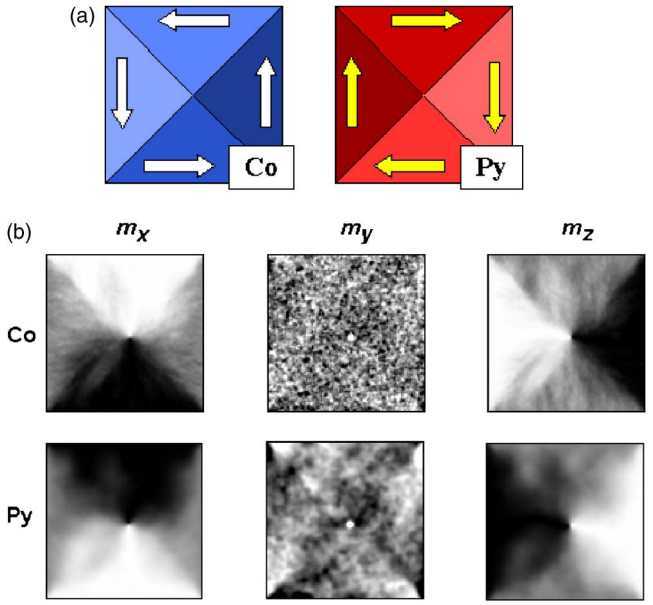

FIG. 10. (Color online) Static equilibrium magnetization state for $H_{ext}=0$ for the same Co/Cu/Py element, as shown in Fig. 7 [starting from Landau magnetization states with opposite rotation senses in Co and Py layers—see (a)], but with the Co layer having a hcp polycrystalline structure with the uniaxial grain anisotropy $K_{un}=4\times10^6$ ergs/cm^3. Due to such a large random anisotropy value, the symmetry of the final magnetization state is strongly disturbed (b) and boundary regions between the domains are very wide.

E. Trilayer Co/Cu/Py element: Influence of the Co anisotropy type

It is well known that thin polycrystalline Co films may possess two kinds of the magnetocrystalline grain anisotropy, according to the two possible grain types: fcc grains have the cubic anisotropy $K_{cub}^{Co}=6\times10^5$ ergs/cm^3 (the case which was analyzed above) and hcp grains have the much stronger uniaxial anisotropy $K_{un}^{Co}=4\times10^6$ ergs/cm^3 (see Ref. 19 and original experiments in Ref. 26 for the corresponding discussion). Films with mixed fcc-hcp structure are also possible. For this reasons, we have studied the effect of the Co anisotropy type on the equilibrium magnetization structure and magnetization dynamics of our trilayer simulating the system with all parameters as given above, and with the starting Landau states with the same rotation sense in both magnetic layers, but with the uniaxial anisotropy of Co grains $K_{un}^{Co}=4\times10^6$ ergs/cm^3. Grain anisotropy axes were again distributed randomly in 3D. Corresponding results are presented in Figs. 10 and 11.

The major effect of such a large magnetocrystalline grain anisotropy is the strong disturbance of the equilibrium magnetization structure, as it can be seen from Fig. 10. Despite the small average grain size $\langle D\rangle=10$ nm, the anisotropy fluctuations in Co even after their averaging out[25] are sufficiently strong to induce large deviations from the ideal Landau structure and to enforce significant randomly varying out-of-plane magnetization component on the lateral Co surfaces. The stray field induced on the Py layer by this $m_\perp^{Co}(\mathbf{r})$ component nearly destroys the original Landau magnetization structure of this layer so that only the overall magnetization rotation sense is preserved. The initially triangular domains of the Landau structure now have a highly irregular form and only small pieces of domain walls (mainly near the Py square corners) can be recognized [Fig. 10(b)].

Correspondingly, the magnetization dynamics of such a trilayer element again differs qualitatively from all cases studied above (Fig. 11). Oscillations of the domain walls are almost invisible. Average magnetization time dependence is entirely dominated by the circular wave emitted from the central vortex, as shown in Figs. 11(b) and 11(c). Due to the strongly disturbed domain structure and absence of well defined domain walls (at least in the middle of the Py square), the wave front is roughly circular from the very beginning. However, irregularities of the equilibrium magnetization structure within the domains lead to large modulations of the oscillation amplitude along the wave front, as it can be recognized already for the initial stage of the wave propagation [Fig. 11(b)].

III. VERIFICATION OF SIMULATION PREDICTIONS AND COMPARISON WITH EXPERIMENTAL OBSERVATIONS

Although, as already mentioned in the Introduction, both static magnetization structures and magnetization dynamics in multilayer nanoelements have been extensively studied in

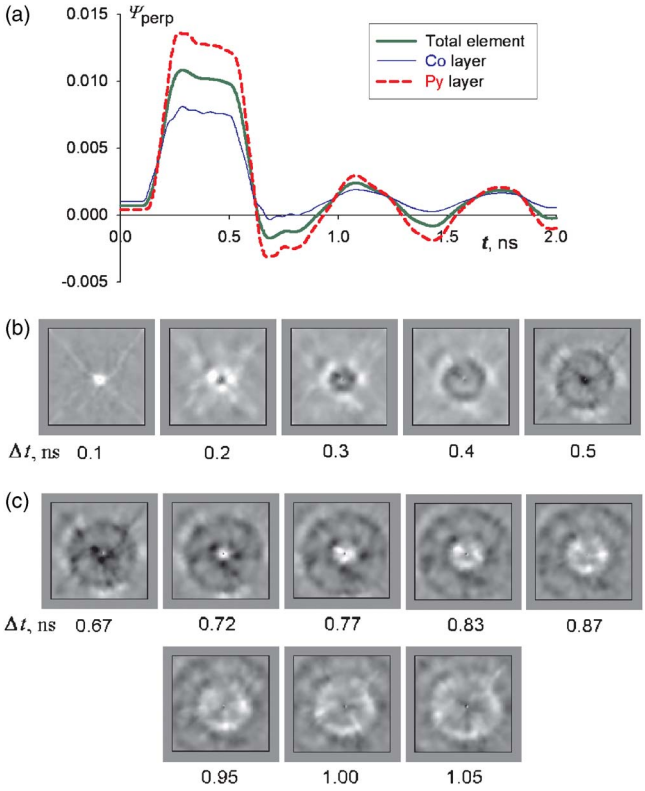

FIG. 11. (Color online) Magnetization dynamics of a trilayer Co/Cu/Py element with the static magnetization structure shown in Fig. 10(b) in the pulsed field presented in the same way as in Fig. 9. Due to the strong disturbance of the static magnetization state, the oscillations of domain walls are nearly invisible. Although the front of the dominating spin wave remains approximately circular, the wave amplitude shows significant inhomogeneities along this wave front.

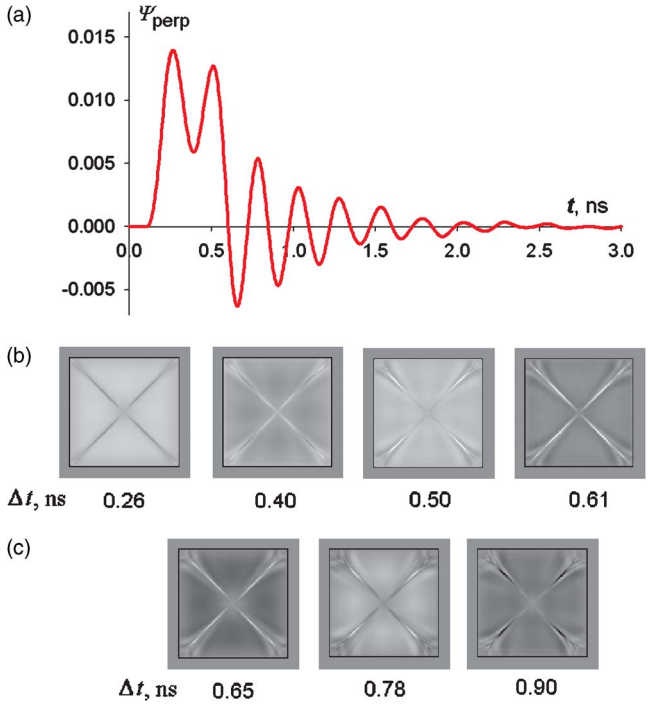

FIG. 12. (Color online) Simulated transient magnetization dynamics for a single-layer Py element with lateral sizes 4×4 mkm^2 and thickness $h_{Py}=50$ nm (after the same field pulse and presented in the same way as in Fig. 3). Strong magnetization oscillations within the domain regions after the field pulse can be seen.

the last several years, we are not aware of any experiments which could be used for direct confirmation or disprove of our simulation results.

In principle, our predictions concerning the equilibrium magnetization structure in square mkm-sized multilayer elements (Figs. 4, 8, 10, and 12) can be verified quite easily. Fabrication of mkm- and sub-mkm patterned multilayer elements of corresponding sizes is possible using several experimental techniques. Deformation of the normal Landau structure predicted by us is strong enough for both the same and opposite magnetization rotation senses in individual layers of the magnetic element. Hence, it should be possible to detect this deformation with the state-of-the-art methods for the observation of magnetization structures in nanometer-thick layers, e.g., using the meanwhile standard high-resolution MFM facilities. We believe, that in an array of square nanoelements composed, as described in this paper, both types of the equilibrium magnetization states (depending on random initial fluctuations of the magnetization) will be formed so that structures shown both in Figs. 4 and 7 can be found.

Magnetization *dynamics* of thin film systems can be measured nowadays not only with a very high lateral and temporal resolution but also element specific using the synchrotron x-ray radiation[24,27,28] with the potential resolution of several tens of nanometers. Layer-selective measurements are also possible using the Kerr microscopy technique,[29] whereby the resolution lies in the sub-mkm region (see, e.g., the recent detailed study of the magnetization dynamics of the Landau state for Py squares with sizes of ~10–40 mkm in Ref. 30). As already mentioned in the Introduction, most papers on this topic are devoted to the magnetization dynamics of mkm-sized *single-layer* elements. Excitations for trilayered *circular* Py/Cu/Py nanodots at different external fields were studied in thermodynamical equilibrium in Ref. 31; mainly the interlayer interaction effects due to the magnetic poles on the *edges* of nearly saturated layers have been described. There are also a few papers where the magnetization *switching* of rectangular magnetic trilayers is studied (see, e.g., Ref. 32), where the major effect is also due to the strong stray fields induced near the edges of a nanoelement in a magnetically saturated state.

We are aware of only two experimental studies which results can be more or less directly related to the subject of this paper, namely, the interlayer dipolar interaction dominated by the nearly in-plane domain walls of the closed (Landau-like) magnetization configuration. In both cases[24,27] the magnetization dynamics of Co/Cu/Py square trilayers was studied using the element-specific time-dependent synchrotron x-ray microscopy.

In the pioneering paper,[24] the transient magnetization dynamics of a relatively large 4×4 mkm^2 trilayer Co (50 nm)/Cu (2 nm)/Py (50 nm) was studied by the pump-and-probe x-ray magnetic circular dichroism (XMCD) microscopy in the field pulse perpendicular to the sample plane. This technique has allowed to investigate the magnetization dynamics with the temporal resolution ~50 ps and potential spatial resolution ~20 nm (however, the actual res-

olution achieved in Ref. 24 is much poorer and is difficult to estimate due to a significant shot noise). Stoll *et al.*[24] did not study the equilibrium magnetization state of their system and have presented spatial maps of the out-of-plane magnetization component of the Py layer only for various time moments during and after the field pulse. Magnetization maps shown in Ref. 24 are effectively differential images between the excited and equilibrium magnetic states, so that the contrasts due to the *static* domain walls and central vortex of the closed magnetization structure are excluded.

The main qualitative features of experimental images presented in Ref. 24 are the following: (i) bright and relatively narrow bands along the diagonals of the squared magnetic element, i.e., where the domain walls of the normal equilibrium Landau pattern are located; (ii) at the same time different domain walls exhibit contrast of *different brightnessess* and even of *different signs*, indicating that oscillations phases and/or frequencies for different walls are different; (iii) after the decay of the field pulse virtually *no contrast within the domains* themselves can be seen, so that the average out-of-plane magnetization component after the field pulse is zero ($\langle m_{\perp}^{\mathrm{Py}}(\mathbf{r})\rangle = 0$) within the experimental resolution.

The authors of Ref. 24 attributed the narrow contrast bands mentioned above to the domain walls oscillations. To support their experimental findings, Stoll *et al.* have performed dynamic micromagnetic simulations, where they have included the *Py layer only* and discretized this layer only in the lateral plane. Simulated out-of-plane magnetization images shown in Ref. 24 demonstrate, of course, the time-dependent contrast between the oscillations of domain walls and domains themselves, but clearly fail to reproduce all other qualitative features of their experimental images listed above.

We have also performed simulations of the Py single layer element with the sizes used in Ref. 24 discretizing it into $400\times400\times4$ (totally 6.4×10^5) cells. We note that due to the low anisotropy and relatively low saturation magnetization of Py the size of our discretization cells $10\times10\times12.5$ nm^3 was small enough to reproduce main features of the Py dynamics. Proper simulation of the magnetic trilayer with the same lateral sizes including the 50 nm thick Co layer would require to halve the cell size in each dimension so that the overall cell number would be prohibitively large for the state-of-the-art micromagnetic simulations. Our $m_{\perp}^{\mathrm{Py}}(\mathbf{r})$ images (Fig. 12) qualitatively agree with simulation data from Ref. 24, demonstrating once more that when the interaction with the Co layer is neglected, *in-phase* oscillations of all four DWs of the Landau pattern should be observed. In addition, the strong contrast within the domains after the field pulse is clearly seen in Fig. 12(c), manifesting itself also in strong after-pulse oscillations of the *average* out-of-plane magnetization $\langle m_{\perp}^{\mathrm{Py}}(t)\rangle$, as shown in Fig. 12(a). The amplitude of these after-pulse oscillations is comparable with the maximal value of $\langle m_{\perp}^{\mathrm{Py}}\rangle$ achieved during the pulse. Taking into account that the domain contrast during the pulse is clearly seen in the experimental images presented in Ref. 24, it is unlikely that approximately the same contrast after the pulse would be completely overlooked. All in one, experimental findings from Ref. 24 cannot be explained satisfactory when the dynamics of Co layer and the interlayer interaction in the trilayer Co/Cu/Py is neglected.

Taking into account that we could not simulate (at least not with proper resolution) the complete system studied in Ref. 24, we can compare the results of Stoll *et al.* with our simulation data only qualitatively. First of all, we note that the straight lines corresponding to the domain wall oscillations indicate that Co and Py layers in this experiment possess Landau magnetization states with opposite rotation senses because for the trilayer with the same magnetization rotation senses in both magnetic layers domain walls should be strongly bended (see Figs. 4 and 6 above).

From the remaining possibilities, dynamic magnetization images of the trilayer with "opposite" Landau patterns and fcc Co crystallites (Fig. 9) demonstrate well pronounced straight lines corresponding to the domain wall oscillations similar to those observed in Ref. 24. However, due to the high symmetry of the equilibrium state, all domain walls oscillate in phase and with the same amplitude, in contrast with strongly out-of-phase DW oscillations with different amplitudes seen in Fig. 2 from Ref. 24. For the same trilayer with hcp-Co magnetization dynamics images are asymmetric (Fig. 11), but due to the very blurred boundaries between Py domains virtually no contrast is observed along the square diagonals (which would correspond to DW oscillations).

At this point it should be noted that the thickness of magnetic layers studied in Ref. 24 ($h_{\mathrm{Co}}=h_{\mathrm{Py}}=50$ nm) is twice as large as in our simulated system ($h_{\mathrm{Co}}=h_{\mathrm{Py}}=25$ nm). In a system with such thick layers, domain wall structure disturbed due to the interlayer interaction, could be partially recovered due to thicker magnetic layers. To check this idea, we have simulated the Co/Cu/Py trilayer with the same parameters and initial magnetization structure, as for the system shown in Figs. 10 and 11, but with the Py thickness $h_{\mathrm{Py}}=50$ nm; here, the Py layer was discretized in eight in-plane sublayers so that the size of the discretization cell was preserved. Corresponding simulation results are shown in Figs. 13 (equilibrium state) and 14 (magnetization dynamics). One can see, that for such increased Py thickness domain walls in the equilibrium magnetization state are, indeed, partially recovered (see Fig. 13) so that their oscillations are clearly visible in the dynamic patterns (Fig. 14). Due to the remaining asymmetry of the magnetization structure, oscillations of different DWs have different spatial patterns, amplitudes, and frequencies in a qualitative agreement with the images displayed in Ref. 24. The average out-of-plane magnetization projection exhibits only very weak oscillations after the field pulse, which is also in agreement with Ref. 24. However, we observe significant magnetization contrast near the square center which is due to the wave emitted by the vortex core; this contrast was not found experimentally.[24]

In the second paper mentioned above,[27] the magnetization dynamics of 1×1 mkm^2 Co (20 nm)/Cu (10 nm)/Py (20 nm) trilayer was studied in the *in-plane* pulsed magnetic field so that mainly the central vortex motion could be seen both in Co and Py layers. The authors display also the equilibrium magnetization structures of both

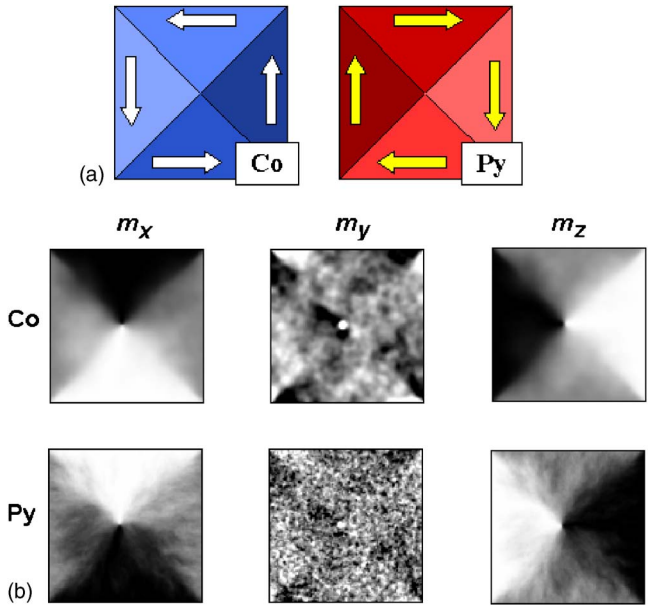

FIG. 13. (Color online) Static equilibrium magnetization state for $H_{ext}=0$ for the same Co/Cu/Py element, as shown in Fig. 10 [starting from Landau states with opposite rotation senses in Co and Py layers—see (a)], but with the thicker Py layer: $h_{Py}=50$ nm. Due to the increased Py layer thickness, domain walls within this layer are partially recovered [see the gray-scale map of $m_y(\mathbf{r})$ for Py in (b)].

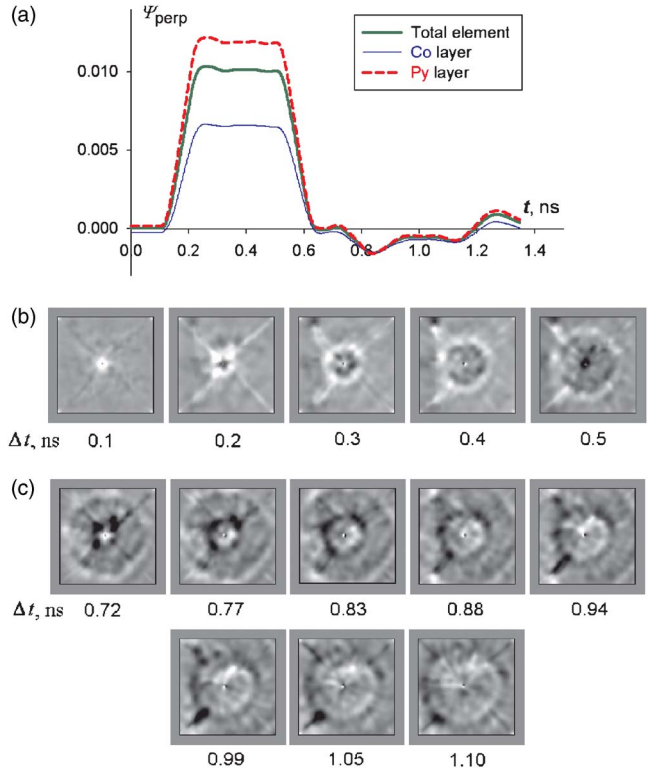

FIG. 14. (Color online) Magnetization dynamics of a trilayer Co/Cu/Py element with the static magnetization state from Fig. 13(b) presented in the same way as in Fig. 11. In contrast to the case shown in Fig. 11, oscillations of domain walls can be clearly seen. However, these oscillations remain strongly asymmetric, what can be seen especially well on the magnetization maps after the field pulse (c).

magnetic layers (see Fig. 1 in Ref. 27), also obtained using XMCD microscopy. Unfortunately, the resolution of these images is still not good enough to make any quantitative statements, so one can only say that both Co and Py layers possess closed magnetization structures with the same rotation senses and that these structures are somewhat disturbed (compared to "ideal" Landau patterns). However, no meaningful quantitative comparison to our results presented in Fig. 4 is possible.

IV. CONCLUSION

In this paper, we have studied the effects of magnetodipolar interlayer interaction in trilayer elements with lateral sizes in sub-mkm region and magnetic layers and spacer thicknesses of several nanometers. We have shown that due to such a small interlayer distance even relatively weak stray field induced by the 90° Néel domain walls of the *closed magnetization state* (Landau-like pattern) causes qualitative changes of both the equilibrium magnetization structure and magnetization dynamics in these systems. We have also demonstrated that the effect of such an interaction may be very different, depending not only on the initial magnetization state used to find the equilibrium magnetization pattern of a system, but also on the crystallographic structure of magnetic layers. This random crystal grain structure significantly affects the magnetization dynamics also for very small crystallite size, where the random magnetocrystalline anisotropy of the grains is largely averaged out. The statement about this anisotropy averaging is often used to justify the neglect of this random anisotropy when simulating the corresponding magnetization dynamics; our results reveal that in many important cases such a neglect may be the prohibitive oversimplification of a problem.

Our simulations clearly demonstrate that for the qualitative and especially quantitative understanding of magnetization dynamics in multilayers, magnetodipolar interlayer interaction effects must be included into consideration, even when the equilibrium magnetization structure forms a closed flux state and thus its stray field is believed to be relatively weak.

Although we are not aware of any experimental studies which results could be directly compared to our simulation data, our main predictions can be relatively easily verified with available experimental techniques, as discussed in detail in Sec. III. However, the accurate sample characterization both from crystallographic and magnetic points of view is required to enable a meaningful comparison with experimental results.

ACKNOWLEDGMENTS

The authors acknowledge fruitful discussions with P. Fischer and A. Slavin. This research was partly supported by the Deutsche Forschungsgemeinschaft (DFG Grant No. BE 2464/4-1).

[1] *Magnetic Multilayers and Giant Magnetoresistance: Fundamentals and Industrial Applications*, Springer Series in Surface Sciences Vol. 37, edited by U. Hartmann (Springer, New York, 2000); *Magnetic Microscopy of Nanostructures*, Series: NanoScience and Technology, edited by H. Hop-

ster and H. P. Oepen (Springer, New York, 2005); *Magnetic Heterostructures: Advances and Perspectives in Spinstructures and Spintransport*, Springer Tracts in Modern Physics Vol. 227, edited by H. Zabel and S. D. Bader (Springer, New York, 2007).
[2]C. Bayer, J. Jorzick, B. Hillebrands, S. O. Demokritov, R. Kouba, R. Bozinoski, A. N. Slavin, K. Guslienko, D. V. Berkov, N. L. Gorn, and M. P. Kostylev, Phys. Rev. B **72**, 064427 (2005).
[3]R. D. McMichael and M. D. Stiles, J. Appl. Phys. **97**, 10J901 (2005).
[4]V. V. Kruglyak, P. S. Keatley, R. J. Hicken, J. R. Childress, and J. A. Katine, J. Appl. Phys. **99**, 08F306 (2006).
[5]J. Podbielski, F. Giesen, and D. Grundler, Phys. Rev. Lett. **96**, 167207 (2006).
[6]M. Buess, T. Haug, M. R. Scheinfein, and C. H. Back, Phys. Rev. Lett. **94**, 127205 (2005); G. Gubbiotti, G. Carlotti, T. Okuno, M. Grimsditch, L. Giovannini, F. Montoncello, and F. Nizzoli, Phys. Rev. B **72**, 184419 (2005); K. Yu. Guslienko, W. Scholz, R. W. Chantrell, and V. Novosad, *ibid.* **71**, 144407 (2005); X. Zhu, Z. Liu, V. Metlushko, P. Grütter, and M. R. Freeman, *ibid.* **71**, 180408 (2005); G. Gubbiotti, M. Madami, G. Carlotti, H. Tanigawa, T. Ono, L. Giovannini, F. Montoncello, Phys. Rev. Lett. **97**, 247203 (2006); K. Yu. Guslienko, X. F. Han, D. J. Keavney, R. Divan, and S. D. Bader, Phys. Rev. Lett. **96**, 067205 (2006); I. Neudecker, K. Perzlmaier, F. Hoffmann, G. Woltersdorf, M. Buess, D. Weiss, and C. H. Back, Phys. Rev. B **73**, 134426 (2005).
[7]K. Perzlmaier, M. Buess, C. H. Back, V. E. Demidov, B. Hillebrands, and S. O. Demokritov, Phys. Rev. Lett. **94**, 057202 (2005).
[8]M. Wolf, U. K.Röβler, and R. Schäfer, J. Magn. Magn. Mater. **314**, 105 (2007).
[9]J. Raabe, C. Quitmann, C. H. Back, F. Nolting, S. Johnson, and C. Buehler, Phys. Rev. Lett. **94**, 217204 (2005).
[10]M. Yan, G. Leaf, H. Kaper, R. Camley, and M. Grimsditch, Phys. Rev. B **73**, 014425 (2006).
[11]M. Bolte, G. Meier, and C. Bayer, Phys. Rev. B **73**, 052406 (2006).
[12]W. Kuch, *Magnetic Imaging*, Lecture Notes Physics Vol. 697(Springer-Verlag, Berlin Heidelberg, 2006) p. 275.
[13]K. S. Buchanan, K. Yu. Guslienko, A. Doran, A. Scholl, S. D. Bader, and V. Novosad, Phys. Rev. B **72**, 134415 (2006).
[14]A. Hubert and R. Schäfer, *Magnetic Domains: The Analysis of Magnetic Microstructures* (Springer Verlag, Heidelberg, 1998).
[15]L. Thomas, M. G. Samant, and S. S. P. Parkin, Phys. Rev. Lett. **84**, 1816 (2000).
[16]W. S. Lew, S. P. Li, L. Lopez-Diaz, D. C. Hatton, and J. A. C. Bland, Phys. Rev. Lett. **90**, 217201 (2003).
[17]V. Christoph and R. Schäfer, Phys. Rev. B **70**, 214419 (2004).
[18]J. Vogel, W. Kuch, R. Hertel, J. Camarero, K. Fukumoto, F. Romanens, S. Pizzini, M. Bonfim, F. Petroff, A. Fontaine, and J. Kirschner, Phys. Rev. B **72**, 220402(R) (2005).
[19]D. V. Berkov and N. L. Gorn, Phys. Rev. B **72**, 094401 (2005).
[20]D. V. Berkov and N. L. Gorn, MICROMAGUS—package for micromagnetic simulations (http:\\www.micromagus.de).
[21]Y. Tserkovnyak, A. Brataas, G. E. W. Bauer, and B. I. Halperin, Rev. Mod. Phys. **77**, 1375 (2005).
[22]D. V. Berkov and N. L. Gorn, J. Magn. Magn. Mater. **290–291P1**, 442 (2005).
[23]M. Grimsditch, L. Giovannini, F. Montoncello, F. Nizzoli, G. K. Leaf, and H. G. Kaper, Phys. Rev. B **70**, 054409 (2004).
[24]H. Stoll, A. Puzic, B. van Waeyenberge, P. Fischer, J. Raabe, M. Buess, T. Haug, R. Höllinger, C. Back, D. Weiss, and G. Denbeaux, Appl. Phys. Lett. **84**, 3328 (2004).
[25]G. Herzer, in *Nanocrystalline Soft Magnetic Alloys*, Handbook of Magnetic Materials Vol. 10, edited by K. Buschov (Elsevier Science, 1997).
[26]D. Weller, G. R. Harp, R. F. C. Farrow, A. Cebollada, and J. Sticht, Phys. Rev. Lett. **72**, 2097 (1994); R. M. Osgood III, K. T. Riggs, A. E. Johnson, J. E. Mattson, C. H. Sowers, and S. D. Bade, Phys. Rev. B **56**, 2627 (1997); K. Heinz, S. Müller, and L. Hammer, J. Phys.: Condens. Matter **11**, 9437 (1999); J. Langer, R. Mattheis, B. Ocker, W. Mass, S. Senz, D. Hesse, and J. Kräusslich, J. Appl. Phys. **90**, 5126 (2001).
[27]K. W. Chou, A. Puzic, H. Stoll, G. Schütz, B. van Waeyenberge, T. Tyliszczak, K. Rott, G. Reiss, H. Brückl, I. Neudecker, D. Weiss, and C. H. Back, J. Appl. Phys. **99**, 08F305 (2006).
[28]Y. Guana, W. E. Bailey, C.-C. Kao, E. Vescovo, and D. A. Arena, J. Appl. Phys. **99**, 08J305 (2006).
[29]R. Schäfer, R. Urban, D. Ullmann, H. L. Meyerheim, B. Heinrich, L. Schultz, and J. Kirschner, Phys. Rev. B **65**, 144405 (2002).
[30]A. Neudert, J. McCord, D. Chumakov, R. Schäfer, and L. Schultz, Phys. Rev. B **71**, 134405 (2005).
[31]G. Gubbiotti, M. Madami, S. Tacchi, G. Carlotti, and T. Okuno, Phys. Rev. B **73**, 144430 (2006).
[32]J. X. Zhang and L. Q. Chen, J. Appl. Phys. **97**, 084313 (2005).